International Journal of Fracture **129:** 199–220, 2004.

Fracture analysis in the conventional theory of mechanism-based strain gradient (CMSG) plasticity

S. QU[1], Y. HUANG[1,*], H. JIANG[1], C. LIU[2], P.D. WU[3] and K.C. HWANG[4]
[1]*Department of Mechanical and Industrial Engineering, University of Illinois, Urbana, IL 61801, U.S.A.*
[2]*Materials Science and Technology Division, Los Alamos National Laboratory, Los Alamos, NM 87545, U.S.A.*
[3]*Alcan International Limited, Kingston Research and Development Center, Kingston, Ontario K7L 5L9, Canada*
[4]*Department of Engineering Mechanics, Tsinghua University, Beijing 100084, China*
[*]*Author for correspondence (E-mail: huang9@uiuc.edu)*

Received 16 November 2003; accepted in revised form 26 April 2004

Abstract. In a remarkable series of experiments, Elssner et al. (1994) and Korn et al. (2002) observed cleavage cracking along a bimaterial interface between Nb and sapphire. The stress required for cleavage cracking is around the theoretical strength of the material. Classical plasticity models fall short to reach such a high stress level. We use the conventional theory of mechanism-based strain gradient plasticity (Huang et al., 2004) to investigate the stress field around the tip of an interface crack between Nb and sapphire. The tensile stress at a distance of 0.1 μm to the interface crack tip reaches $13.3\sigma_Y$, where σ_Y is the yield stress of Nb. This stress is nearly 4 times of that predicted by classical plasticity theory ($3.6\sigma_Y$) at the same distance to the crack tip, and is high enough to trigger cleavage cracking in materials and interfaces. This is consistent with Elssner et al.'s (1994) and Korn et al.'s (2002) experimental observations.

Key words: Cleavage cracking, interface fracture, strain gradient plasticity, Taylor dislocation model.

1. Introduction

1.1. Cleavage cracks in presence of plastic flow

In a remarkable series of experiments, Elssner et al. (1994) and Korn et al. (2002) measured both the macroscopic fracture toughness and atomic work of separation of an interface between single crystal niobium and sapphire. The macroscopic work of fracture, measured from a four-point bend specimen, was about 1000 times higher than the atomic work of separation obtained from the equilibrium shapes of microscopic pores on the interface. This large difference between macroscopic and atomic work of fracture was attributed to plastic dissipation in niobium, i.e., the significant plastic flow associated with dislocation activities. It is anticipated that the crack tip would be blunted by dislocations in niobium, and the maximum stress around the crack tip is no more than 4 to 5 times the tensile yield stress σ_y of niobium according to classical plasticity models (Hutchinson, 1997). However, Elssner et al. (1994) and Korn et al. (2002) observed cleavage cracks in the niobium/sapphire system, i.e., the crack tip remained atomistically sharp without any blunting even though niobium had a large number of dislocations. Cleavage cracks in presence of significant plastic flow have also been observed in many other material systems (e.g., Oh et al., 1987; Wang and Anderson, 1991; Beltz and Wang, 1992; Korn et al., 1992; O'Dowd et al, 1992; Bagchi et al., 1994; Bagchi and Evans, 1996). The stress level around a cleavage crack tip for atomic decohesion of a lattice or strong interface is the theoretical strength of the metal, which is about one tenth of the shear

modulus, $\mu/10$. For typical metals, it is approximately $E/30$ (E is the Young's modulus) or 10 times the yield stress, i.e., $10\sigma_y$. This stress level of $10\sigma_y$ required for cleavage cracks is more than twice the maximum stress around the crack tip predicted by classical plasticity models. It is clear that classical plasticity models fall short to explain Elssner et al.'s (1994) and Korn et al.'s (2002) experimental observation of cleavage cracks in presence of plastic flow.

There are significant efforts to develop continuum (but not classical) plasticity models that predict higher stress level around the crack tip than classical plasticity models do in order to explain the observed cleavage cracks in presence of significant plastic flow. Suo et al. (1993) introduced the so-called SSV model in which the crack tip was surrounded by a dislocation-free strip. The strip was elastic (since there are no dislocations inside), with the strip height on the order of dislocation spacing. The strip was in turn surrounded by the plastic zone. The SSV model indeed predicted much higher stress around the crack tip in the elastic strip. Using the self-consistent method, Beltz et al. (1996) determined the height of the dislocation-free strip. Wei and Hutchinson (1999) combined the SSV model with the cohesive zone model (e.g., Needleman, 1987; Tvergaard and Hutchinson, 1992, 1993; Xu and Needleman, 1994; Camacho and Ortiz, 1996) to investigate the stress level around a crack tip.

1.2. Strain gradient plasticity theories

An alternative approach to study cleavage cracks in presence of significant plastic flow comes from strain gradient plasticity theories. These theories are developed primarily to study size effects observed in materials at the micron and sub-micron scales, such as the micro-indentation hardness experiments of various metallic materials (e.g., Nix, 1989, 1997; de Guzman et al., 1993; Stelmashenko et al., 1993; Atkinson, 1995; Ma and Clarke, 1995; Poole et al., 1996; McElhaney et al., 1998; Suresh et al., 1999; Saha et al., 2001; Tymiak et al., 2001; Swadener et al., 2002; Lou et al., 2003); micro-twist experiments of thin copper wires (Fleck et al., 1994); micro-bend experiments of nickel foils (Stolken and Evans, 1998; Shrotriya et al., 2003) and aluminum beams (Haque and Saif, 2003); particle reinforced metal matrix composites (Lloyd, 1994; Argon et al., 1998); micro-electro-mechanical systems (Douglass, 1998); and discrete dislocation models of van der Giessen, Needleman and co-workers (e.g., Needleman et al., 2001; van der Giessen et al., 2001; Shi et al., 2004a, b). These size effects, which cannot be explained by classical plasticity models that possess no internal material lengths, have been attributed to geometrically necessary dislocations associated with non-uniform plastic deformation. Accordingly, strain gradient plasticity theories have been developed, and internal material lengths are introduced to scale with strain gradients from the dimensional consideration.

The strain gradient plasticity theories can be classified to the lower-order and higher-order theories. The higher-order theories involve the rate of strain gradient in the incremental constitutive relation (e.g., Fleck and Hutchinson, 1993, 1997, 2001; Fleck et al., 1994; Gao et al., 1999a, b; Huang et al., 2000a, b; Qiu et al., 2001, 2003; Gurtin, 2002; Hwang et al., 2002, 2003). They belong to Mindlin's (1964) theoretical framework of higher-order continuum theory, and require additional governing equations and additional boundary conditions beyond those in the classical continuum theories. For the lower-order theories, the plastic strain gradient comes into play via the incremental plastic work hardening modulus. The lower-order theories involve the conventional stress and strain only, and require no additional boundary conditions beyond those in the classical continuum theories (e.g., Acharya and Bassani, 2000; Acharya and Beaudoin, 2000; Bassani, 2001; Beaudoin et al., 2001; Evers et al., 2002; Huang

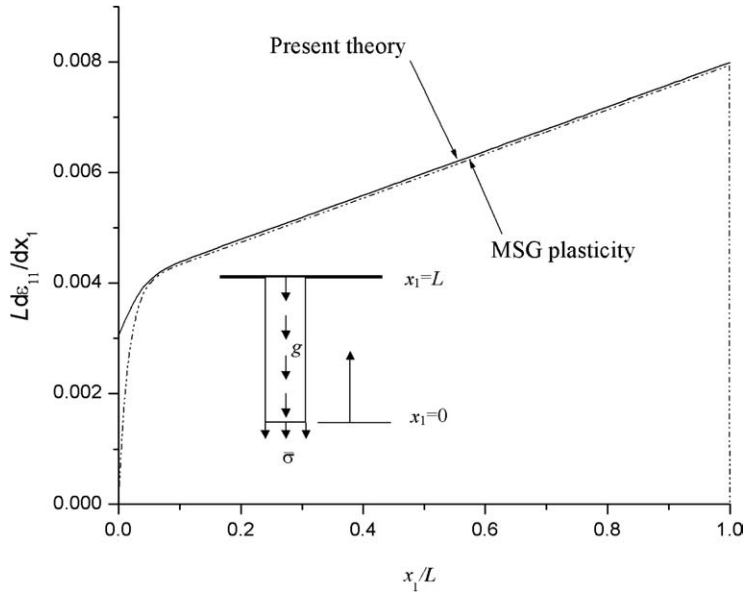

Figure 1. The strain gradient distribution $d\varepsilon_{11}/dx_1$ in the bar of length $L = 0.1l$ predicted by lower-order theory (CMSG, solid curve) and MSG plasticity, higher-order strain gradient plasticity theory (dashed curve) for a bar subject to body force and applied stress traction at the free end, where l is the intrinsic material length in strain gradient plasticity. The material parameters are power-law hardening exponent $N = 0.5$, Poisson's ratio $\nu = 1/2$, the ration of yield stress to Young's modulus $\sigma_Y/E = 0.2\%$, and rate sensitivity exponent $m = 20$.

et al., 2004). Volokh and Hutchinson (2002) provided a critical evaluation of Bassani's (2001) lower-order strain gradient plasticity theories, and pointed out that the lower-order theory is not actually lower order. Rather some higher-order boundary conditions are imposed implicitly through the numerical evaluation of the plastic strain gradient. For a strip subject to pure shear, Niordson and Hutchinson (2003) showed that the plastic strain distribution predicted by Bassani's (2001) lower-order strain gradient plasticity theory may exhibit a vertex at the center of the strip, which contradicts the symmetry condition at the center. Niordson and Hutchinson's (2003) analysis, however, involves the central difference scheme inside the strip and skew difference scheme on the strip boundary. In order to avoid this complexity of using different numerical schemes by Niordson and Hutchinson (2003), Yun et al. (2004) used the method of characteristics to determine the 'domain of determinacy' for the same problem of a strip subject to pure shear. They established that, as the applied shear stress increases, the 'domain of determinacy' shrinks and eventually vanishes. Additional, non-classical boundary conditions are necessary for the well-posedness of Bassani's (2001) lower-order strain gradient plasticity theory. Within the 'domain of determinacy', Yun et al.'s (2004) solution based on the method of characteristics agrees well with Niordson and Hutchinson's (2003) finite difference solution. Outside the 'domain of determinacy' the solution is not unique unless additional, non-classical boundary conditions are imposed. Acharya et al. (2004) also examined the same problem of a strip in pure shear, but used Acharya and Bassani's (2000) lower-order theory. They established that the necessity of additional, non-classical boundary conditions depends on the hardening function and the initial strain distribution. It is possible for Acharya and Bassani's (2000) lower-order theory no additional boundary conditions are necessary.

Huang et al. (2004) compared the higher-order (Gao et al., 1999b; Huang et al., 2000a, b; Qiu et al., 2003) and lower-order strain gradient plasticity theories (Huang et al., 2004) based on the same dislocation model (Taylor, 1934, 1938). They studied five examples including uniaxial tension with a constant body force, strip in pure shear, bending, torsion, and void growth, and found that the stress (or strain) fields predicted by the higher-order and lower-order theories are identical except in a thin boundary layer of the solid. This boundary layer results from the higher-order boundary conditions and the thickness of boundary layer is on the order of 10 nm. For a bar of length L subject to body force and applied stress traction (at the free end of the bar), the strain gradient distributions given by both lower-order (Huang et al., 2004) and higher-order strain gradient plasticity theories (Gao et al., 1999b; Huang et al., 2000a) based on the same dislocation model (Taylor, 1934, 1938) are shown in Figure 1. The modeling parameters can be found in Huang et al. (2004) [also Shi et al. (2001)]. It is clearly observed that the lower-order and higher-order theories agree very well except within two boundary layers at the ends $x_1 = 0$ and $x_1 = L$. The strain gradient distributions within two boundary layers are significantly different due to the additional boundary conditions in the higher-order theories. Therefore, the higher-order boundary conditions only influence the stress and strain fields near the boundary of the solid.

1.3. The strain gradient effect on fracture of homogeneous materials

The existing fracture analyses in strain gradient plasticity are limited to homogeneous materials. The phenomenological theory of strain gradient plasticity based on the rotation gradients (Fleck and Hutchinson, 1993) does not show a significant increase in the stress level around the stationary crack tip (e.g., Huang et al., 1995, 1997, 1999; Xia and Hutchinson, 1996; Chen et al., 1998). This motivated Fleck and Hutchinson (1997) to introduce stretch gradients in strain gradient plasticity. A much higher stress level is then achieved around the tip of a quasi-static propagating crack (Wei and Hutchinson, 1997), but not around a stationary crack tip (Chen et al., 1999; Shi et al., 2000b). Recently, Jiang et al. (2001) used the higher-order theory of mechanism-based strain gradient plasticity (Gao et al., 1999b; Huang et al., 2000a, b) established from the Taylor dislocation model (1934, 1938) to investigate the stress field around a stationary crack tip in a homogeneous solid. The stress near the crack tip was indeed more than 10 times the yield stress, which was significantly higher than that in the HRR field in classical plasticity (Hutchinson, 1968; Rice and Rosengren, 1968), and might trigger cleavage fracture in ductile materials. Shi et al. (2000a, 2001) investigated the asymptotic crack tip field in the higher-order theory of mechanism-based strain gradient plasticity (Gao et al., 1999b; Huang et al., 2000a, b). They showed that the higher-order boundary conditions have essentially no effect on the stress distribution at a distance of more than 10 nm away from the crack tip. This is consistent with the boundary layer effect discussed in Section 1.2.

1.4. The strain gradient effect on fracture of bimaterial interfaces

The present study aims at investigating the strain gradient effect on fracture of bimaterial interfaces between elastic and elastic-plastic solids. It focuses on the stress increase around the crack tip due to the strain gradient effect, and its implications on cleavage cracking in presence of plastic flow as observed in Elssner et al.'s (1994) and Korn et al.'s (2002) experiments. Since there is essentially no difference between the lower-order and higher-order theories at a distance of more than 10 nm away from the crack tip, we will use the lower-order theory of mechanism-based strain gradient plasticity (Huang et al., 2004) based on the Taylor

dislocation model (1934, 1938). This is because any continuum plasticity theories, including classical and strain gradient plasticity theories, represent the collective behavior of dislocations, and are therefore only applicable at a scale larger than the average dislocation spacing. For a typical dislocation density of 10^{14} m^{-2}, the average dislocation spacing is around 100 nm at which the lower-order (Huang et al., 2004) and higher-order theories of mechanism-based strain gradient plasticity (Gao et al., 1999b; Huang et al., 2000a) give the same stress field. The lower-order theory of strain gradient plasticity is summarized in Section 2, along with the Taylor dislocation model. We begin the fracture analysis for a homogeneous material in Section 3 in order to validate our approach. The interface crack between niobium and sapphire in Elssner et al.'s (1994) 4-point bend specimen is studied in Section 4. The stress around the crack tip is indeed much higher than that predicted by classical plasticity for interface cracks, and it exceeds the stress level for cleavage cracking.

2. A conventional theory of mechanism-based strain gradient plasticity

The conventional theory of mechanism-based strain gradient plasticity (CMSG) developed by Huang et al. (2004) is a lower-order theory based on the Taylor dislocation model (1934, 1938). It is summarized in the following.

2.1. Taylor dislocation model

The shear flow stress τ is related to the dislocation density ρ by (Taylor, 1934, 1938; Bailey and Hirsch, 1960)

$$\tau = \alpha \mu b \sqrt{\rho}, \tag{2.1}$$

where μ is the shear modulus, b is the magnitude of the Burgers vector, and α is an empirical coefficient ranging from 0.3 to 0.5. The dislocation density ρ is composed of the density ρ_S for statistically stored dislocations, which accumulate by trapping each other in a random way (Ashby, 1970), and density ρ_G for geometrically necessary dislocations, which are required for compatible deformation of various parts of the material (Nye, 1953; Cottrell, 1964; Ashby, 1970), i.e.,

$$\rho = \rho_S + \rho_G. \tag{2.2}$$

The density ρ_G is related to the curvature of plastic deformation (Ashby, 1970; Nix and Gao, 1998), or effective plastic strain gradient η^p, by

$$\rho_G = \bar{r} \frac{\eta^p}{b}, \tag{2.3}$$

where $\bar{r}$ is the Nye factor introduced by Arsenlis and Parks (1999) to reflect the effect of crystallography on the distribution of geometrically necessary dislocations, and $\bar{r}$ is around 1.90 for face-centered-cubic (fcc) polycrystals (Arsenlis and parks, 1999; Shi et al., 2004a).

The tensile flow stress σ_{flow} is related to the shear flow stress τ by

$$\sigma_{flow} = M\tau, \tag{2.4}$$

where M is the Taylor factor which acts as an isotropic interpretation of the crystalline anisotropy at the continuum level, and $M = 3.06$ for fcc metals (Bishop and Hill, 1951a, b; Kocks, 1970) as well as for body-centered-cubic metals that slip on {110} planes (Kocks, 1970). The substitution of (2.1)–(2.3) into (2.4) yields

$$\sigma_{flow} = M\alpha\mu b\sqrt{\rho_S + \bar{r}\frac{\eta^p}{b}}. \tag{2.5}$$

For uniaxial tension, the flow stress can also be related to the plastic strain ε^p by $\sigma_{flow} = \sigma_{ref} f(\varepsilon^p)$, where σ_{ref} is a reference stress and f is a nondimensional function determined from the uniaxial stress-strain curve. Since the plastic strain gradient η^p vanishes in uniaxial tension, the density ρ_S of statistically stored dislocations is determined from (2.5) as $\rho_S = \left[\sigma_{ref} f(\varepsilon^p)/(M\alpha\mu b)\right]^2$. The flow stress in (2.5) then becomes

$$\sigma_{flow} = \sqrt{\left[\sigma_{ref} f(\varepsilon^p)\right]^2 + M^2\bar{r}\alpha^2\mu^2 b\eta^p} = \sigma_{ref}\sqrt{f^2(\varepsilon^p) + l\eta^p}, \tag{2.6}$$

where

$$l = M^2\bar{r}\alpha^2\left(\frac{\mu}{\sigma_{ref}}\right)^2 b = 18\alpha^2\left(\frac{\mu}{\sigma_{ref}}\right)^2 b \tag{2.7}$$

is the intrinsic material length in strain gradient plasticity, $M = 3.06$ and $\bar{r} = 1.90$. This intrinsic material length represents a natural combination of the effects of elasticity (shear modulus μ), plasticity (reference stress σ_{ref}) and atomic spacing (Burgers vector b). It is important to note that, even though this intrinsic material length l depends on the choice of the reference stress σ_{ref} in uniaxial tension, the flow stress σ_{flow} in (2.6) does not because the strain gradient term inside the square root in (2.6) becomes $\sigma_{ref}^2 l\eta^p = 18\alpha^2\mu^2 b\eta^p$, and is independent of σ_{ref}. Here the term $18\alpha^2\mu^2 b\eta^p$ involves the plastic strain gradient η^p to be given in Section 2.4, well-defined material properties such as shear modulus and Burgers vector, and the coefficient α in the Taylor dislocation model that varies from 0.3 to 0.5.

2.2. An alternative expression of the uniaxial stress-strain curve

Huang et al. (2004) suggested to rewrite the uniaxial stress-plastic strain relation $\sigma = \sigma_{ref} f(\varepsilon^p)$ to the following viscoplastic expression (e.g., Hutchinson, 1976; Canova and Kocks, 1984; Asaro and Needleman, 1985) in order to pave the way for the establishment of a lower-order theory of CMSG plasticity

$$\dot{\varepsilon}^p = \dot{\varepsilon}_0\left[\frac{\sigma}{\sigma_{ref} f(\varepsilon^p)}\right]^m, \tag{2.8}$$

where $\dot{\varepsilon}^p$ is the rate of plastic strain, $\dot{\varepsilon}_0$ is a reference strain rate, and m is the rate-sensitivity exponent which usually takes a large value ($m \geqslant 20$). In the limit $m \to \infty$, (2.8) degenerates to $\sigma = \sigma_{ref} f(\varepsilon^p)$. Equation (2.8), however, displays a strain-rate sensitivity such that the resulting stress-strain relation depends on the normalized time $\dot{\varepsilon}_0 t$, even though this rate sensitivity is rather weak for a large m ($\geqslant 20$).

Following Kok et al. (2002a, b, c), Huang et al. (2004) proposed to replace the reference strain rate $\dot{\varepsilon}_0$ by the effective strain rate $\dot{\varepsilon}$ in order to eliminate the strain-rate sensitivity. Equation (2.8) then becomes

$$\dot{\varepsilon}^p = \dot{\varepsilon}\left[\frac{\sigma}{\sigma_{ref} f(\varepsilon^p)}\right]m. \tag{2.9}$$

In the limit $m \to \infty$, (2.9) also degenerates to the uniaxial stress-strain relation $\sigma = \sigma_{ref} f(\varepsilon^p)$. Since (2.9) has strain rate on both sides, the resulting stress-strain relation becomes independent of the strain rate, and the strains (including elastic and plastic strains) do not change once

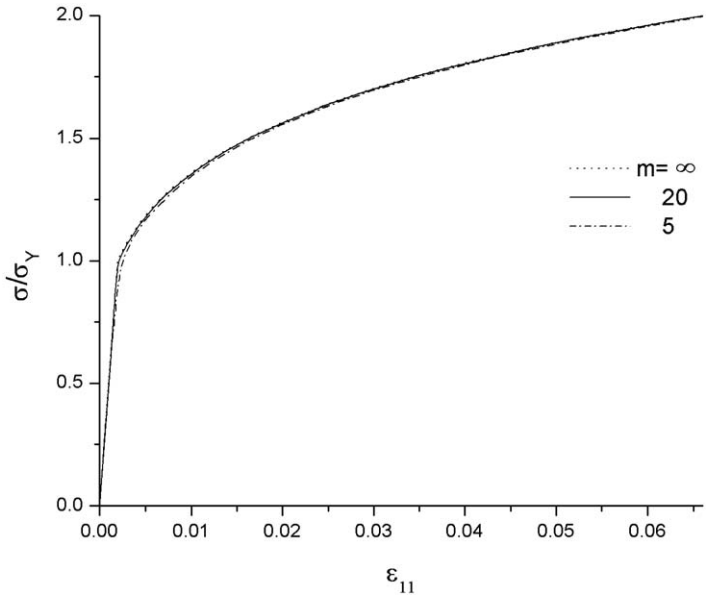

Figure 2. Uniaxial stress-strain relation for rate sensitivity exponent $m = 5, 20$ and ∞; σ_Y is the initial yield stress; power-law hardening exponent $N = 0.2$, the ratio of yield stress to Young's modulus $\sigma_Y/E = 0.2\%$, Poisson's ratio $\nu = 0.3$. The limit $m = \infty$ corresponds to the conventional power-law hardening relation.

the stresses are fixed. Figure 2 shows the uniaxial stress-strain relation for rate sensitivity exponent $m = 5$, 20 and ∞. Other modeling parameters can be found in Huang et al. (2004). It is clearly observed that all curves are very close, and there is essentially no difference between the curves for $m = 20$ and $m = \infty$. Therefore, (2.9) with $m \geqslant 20$ is an excellent representation of the uniaxial stress-strain relation $\sigma = \sigma_{ref} f(\varepsilon^p)$. Even though such an approach looks more complex, it paves the way to establish a conventional theory of strain gradient plasticity based on the Taylor dislocation model, as discussed in the next section.

Another advantage of this approach is that, similar to viscoplastic models, it is not necessary to distinguish elastic unloading from plastic loading any more since (2.9) is applicable to both elastic and plastic deformation. If $\sigma < \sigma_{ref}(\varepsilon^p)$, the plastic strain rate $\dot{\varepsilon}^p$ obtained from (2.9) with $m \geqslant 20$ becomes essentially zero, i.e., the deformation is essentially elastic. Figure 3 shows the loading and unloading stress-strain curve in uniaxial tension. The modeling parameters can be found in Huang et al. (2004). Here $m = \infty$ corresponds to the uniaxial stress-strain relation $\sigma = \sigma_{ref} f(\varepsilon^p)$ and it gives a straight line with the slope of Young's modulus in Figure 3 during unloading. The curve for $m = 20$ is very close to that for $m = \infty$ during both loading and unloading.

2.3. The constitutive model in CMSG plasticity

The volumetric strain rate $\dot{\varepsilon}_{kk}$ and deviatoric strain rate $\dot{\varepsilon}'_{ij}$ in CMSG plasticity are related to the stress rate in the same way as in classical plasticity, i.e.,

$$\dot{\varepsilon}_{kk} = \frac{\dot{\sigma}_{kk}}{3K}, \tag{2.10}$$

$$\dot{\varepsilon}'_{ij} = \frac{\dot{\sigma}'_{ij}}{2\mu} + \frac{3\dot{\varepsilon}^p}{2\sigma_e}\sigma'_{ij}, \tag{2.11}$$

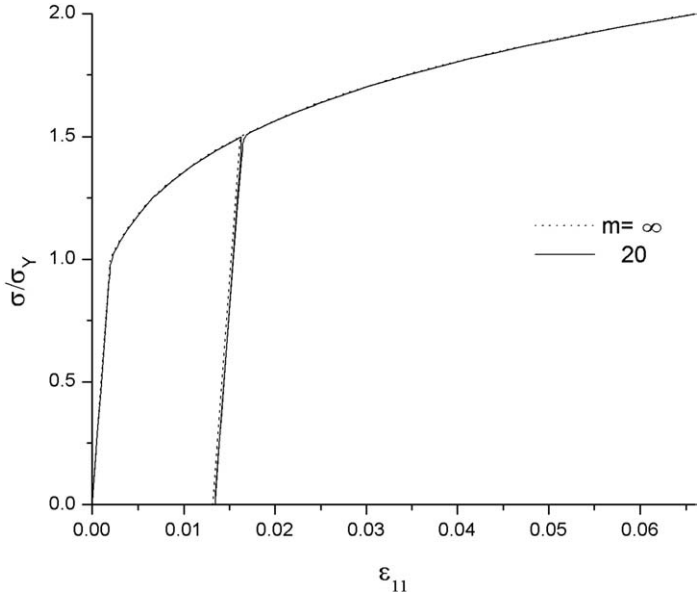

Figure 3. Loading and unloading stress-strain curve in uniaxial tension; σ_Y is the initial yield stress. The stress σ increases monotonically to $1.5\sigma_Y$, at which it unloads completely and reloads to a higher stress $2\sigma_Y$. The material parameters are the same as those in Figure 1. The solid curve ($m = 20$) corresponds to the new constitutive relation (2.9). The dashed curve ($m = \infty$) corresponds to the conventional power-law hardening with a linear unloading relation (a straight line with the slope of Young's modulus E).

where K and μ are the elastic bulk and shear moduli, respectively, σ'_{ij} is the deviatoric stress, and $\sigma_e = \left(3\sigma'_{ij}\sigma'_{ij}/2\right)^{1/2}$ is the effective stress. The effective plastic strain rate $\dot{\varepsilon}^p = \left(2\dot{\varepsilon}^p_{ij}\dot{\varepsilon}^p_{ij}/3\right)^{1/2}$ is obtained from (2.9) except that the tensile flow stress $\sigma_{ref} f\left(\varepsilon^p\right)$ in the denominator is replaced by the flow stress in (2.6) established from the Taylor dislocation model accounting for the strain gradient effect, i.e.,

$$\dot{\varepsilon}^p = \dot{\varepsilon}\left(\frac{\sigma_e}{\sigma_{flow}}\right)^m = \dot{\varepsilon}\left[\frac{\sigma_e}{\sigma_{ref}\sqrt{f^2\left(\varepsilon^p\right) + l\eta^p}}\right]^m, \tag{2.12}$$

where $\dot{\varepsilon} = \left(2\dot{\varepsilon}'_{ij}\dot{\varepsilon}'_{ij}/3\right)^{1/2}$. Equations (2.10)–(2.12) can be rearranged to give the stress rate in terms of the strain rate,

$$\dot{\sigma}_{ij} = K\dot{\varepsilon}_{kk}\delta_{ij} + 2\mu\left\{\dot{\varepsilon}'_{ij} - \frac{3\dot{\varepsilon}}{2\sigma_e}\left[\frac{\sigma_e}{\sigma_{ref}\sqrt{f^2\left(\varepsilon^p\right) + l\eta^p}}\right]^m \sigma'_{ij}\right\}. \tag{2.13}$$

This is the constitutive relation in CMSG, which involves the conventional stress and strain only, and no higher-order stress. The plastic strain gradient comes into play to reduce the incremental plastic modulus, similar to Acharya and Bassani (2000) and Acharya and Beaudoin (2000). CMSG also bears similarity with Ever et al.'s (2002) viscoplastic strain gradient plasticity theory because CMSG would have been viscoplastic if $\dot{\varepsilon}_0$ were not replaced by $\dot{\varepsilon}$ in (2.9). Furthermore, Huang et al. (2004) compared CMSG with the higher-order theory of mechanism-based strain gradient plasticity (Gao et al., 1999b; Huang et al., 2000a, b) established from the same Taylor dislocation model (1934, 1938). The stress distributions

predicted by the lower and higher-order theories are only different within a thin boundary layer whose thickness is around 10nm (e.g., Shi et al., 2001; Huang et al., 2004).

It is important to note that the yield condition $\sigma_e = \sigma_{ref}\sqrt{f^2(\varepsilon^p) + l\eta^p}$ is not strictly enforced in CMSG. Rather it holds approximately via Equations (2.12) or (2.13). The effective stress σ_e is related to the deviatoric stress by $\sigma_e = \left(3\sigma'_{ij}\sigma'_{ij}/2\right)^{1/2}$, and the deviatoric stress is updated via (2.13). The effective strain rate is similarly obtained via $\dot{\varepsilon} = \left(2\dot{\varepsilon}'_{ij}\dot{\varepsilon}'_{ij}/3\right)^{1/2}$.

2.4. Effective plastic strain gradient

There are two measures of effective plastic strain gradient η^p in CMSG (Huang et al., 2004). The first was given by Gao et al. (1999b) who used three quadratic invariants of plastic strain gradient tensor to represent η^p, and the coefficients of three quadratic invariants were determined by three models of geometrically necessary dislocations, namely bending, torsion and void growth. The resulting effective plastic strain gradient is given by

$$\eta^p = \int \dot{\eta} dt,\ \dot{\eta}^p = \sqrt{\frac{1}{4}\dot{\eta}^p_{ijk}\dot{\eta}^p_{ijk}},\ \dot{\eta}^p_{ijk} = \dot{\varepsilon}^p_{ik,j} + \dot{\varepsilon}^p_{jk,i} - \dot{\varepsilon}^p_{ij,k}, \tag{2.14}$$

where $\dot{\varepsilon}^p_{ij}$ is the tensor of plastic strain rate.

Another expression of the effective plastic strain gradient in CMSG results from Nye's dislocation tensor (e.g., Kondo, 1952, 1955; Bilby et al., 1955; Eshelby, 1956; Kröner, 1960; Fox, 1966). Even though the total deformation gradient $\mathbf{F} = \mathbf{F}^e \cdot \mathbf{F}^p$ (Lee, 1969) corresponds to a compatible deformation field, its plastic part $\mathbf{F}^p$ (or equivalently, the inverse elastic part, $\mathbf{F}^{e^{-1}}$) is generally incompatible, and therefore requires geometrically necessary dislocations to accommodate the incompatible plastic deformation (Steinmann, 1996; Arsenlis and Parks, 1999; Shizawa and Zbib, 1999; Acharya and Bassani, 2000; Acharya and Beaudoin, 2000; Beaudoin et al., 2001; Cermelli and Gurtin, 2001). Steinmann (1996) and Cermelli and Gurtin (2001) defined the tensor of geometrically necessary dislocations as $\frac{1}{\det\mathbf{F}^p}\mathbf{F}^p \cdot \left(\nabla \times \mathbf{F}^p\right)$, where det is the determinant and ∇ is the gradient operator. For infinitesimal deformation, it degenerates to $-\boldsymbol{\varepsilon}^p \times \nabla$, where $\boldsymbol{\varepsilon}^p$ is the tensor of plastic strain $\boldsymbol{\varepsilon}^p = \int \dot{\boldsymbol{\varepsilon}}^p dt$. Accordingly, the effective plastic strain gradient η^p is defined as the quadratic invariant of $-\boldsymbol{\varepsilon}^p \times \nabla$, i.e.,

$$\eta^p = \sqrt{(-\boldsymbol{\varepsilon}^p \times \nabla) : (-\boldsymbol{\varepsilon}^p \times \nabla)} = \sqrt{(\boldsymbol{\varepsilon}^p \times \nabla) : (\boldsymbol{\varepsilon}^p \times \nabla)}. \tag{2.15}$$

Huang et al. (2004) examined the difference between two effective plastic strain gradients in (2.14) and (2.15) in several examples, including microbend, microtwist, microvoid growth, uniaxial tension subject to a body force, and an infinite strip in shear. The strain (and stress) fields predicted by CMSG based on these two different effective plastic strain gradients are essentially the same. Therefore, we use (2.14) for the effective plastic strain gradient in the present study.

2.5. Equilibrium equations and boundary conditions

Since CMSG does not involve the higher-order stress, equilibrium equations remain the same as those in conventional continuum theories, i.e.,

$$\sigma_{ji,j} + f_i = 0, \tag{2.16}$$

where f_i is the body force. The traction and displacement boundaries are also the same as their counterparts in conventional continuum theories, i.e.,

$$\sigma_{ji} n_j = t_i, \tag{2.17}$$

$$u_i = \bar{u}_i, \tag{2.18}$$

where n_j is the unit normal, and t_i and $\bar{u}_i$ are stress traction and displacement on the traction boundary and displacement boundary, respectively.

2.6. Limit on CMSG

It is important to note that CMSG as well as other continuum plasticity theories must have lower limits and cannot be applied down to the nanometer scale. This is because the continuum plasticity theories represent the collective behavior of discrete dislocations, and are therefore only applicable at a scale larger than the average dislocation spacing. For example, the Taylor dislocation model (2.1), which represents the collective effect of dislocations on the shear flow stress, holds at a scale larger than the dislocation spacing. For a representative dislocation density $10^{14}/m^2$, the average dislocation spacing is around 100 nm such that the lower limit of CMSG is on the order of 100 nm. This lower limit, however, is not a fixed constant and it may vary for different materials, but such a lower limit exists below which CMSG and other continuum plasticity theories are not applicable. This is similar to the limit of continuum elasticity theory which is not applicable below the atomic spacing.

There is no upper limit of CMSG since the strain gradient term $l\eta^p$ becomes negligible at the large scale. CMSG then naturally degenerates to classical plasticity.

2.7. Finite element analysis for CMSG

Unlike the higher-order theory of mechanism-based strain gradient plasticity (Gao et al., 1999b; Huang et al., 2000a, b), CMSG is a lower-order theory which does not involve the higher-order stress such that its governing equations are essentially the same as those in the classical plasticity. One can easily modify the existing finite element program to incorporate the plastic strain gradient effect. Specifically, we have implemented the constitutive relation (2.13) of CMSG in the ABAQUS finite element program via its USER-MATERIAL subroutine UMAT. Its only difference from classical plasticity is that the plastic strain gradient must be evaluated in UMAT. This is accomplished by the numerical differentiation within the element, i.e., to interpolate the plastic strain increment $\Delta\boldsymbol{\varepsilon}^p$ within each element via the values at Gaussian integration points in the isoparametric space, and then to determine the gradient of plastic strain increment via the differentiation of the shape function.

3. Fracture in homogeneous materials

We use the finite element method for CMSG to investigate the stress field around a plane-strain mode-I crack tip. The crack faces correspond to the rays $\theta = \pm\pi$ in the polar coordinates centered at the tip. A circular region of radius 42 mm centered around the crack tip is analyzed by the finite element method. Very fine mesh is used near the crack tip, around which the smallest element is approximately 10 nm. Only the upper half circular domains is studied due to symmetry, and there are 20 elements in the circumferential direction ($0^\circ \leqslant \theta \leqslant 180^\circ$). The

mesh gradually becomes coarse remote from the crack tip, and the aspect ratio of elements is close to 1. Refined meshes are used to ensure the numerical results are accurate.

The crack faces are traction free. The classical mode-I elastic K field is imposed on the outer boundary ($r = 42\ mm$) of the circular domain surrounding the crack tip. The elastic stress intensity factor K_I of the remote field increases monotonically such that there is no unloading.

The elastic properties of the material include the Young's modulus E and shear modulus μ (or equivalently the Poisson's ratio ν). The stress-plastic strain relation in uniaxial tension can be written as

$$\sigma = \sigma_{ref} f\left(\varepsilon^p\right) = \sigma_Y \left(\frac{E}{\sigma_Y}\right)^N \left(\varepsilon^p + \frac{\sigma_Y}{E}\right)^N, \tag{3.1}$$

which involves the plastic properties: the yield stress σ_Y and plastic work hardening exponent N. The reference stress can be taken as $\sigma_{ref} = \sigma_Y \left(\frac{E}{\sigma_Y}\right)^N$, and $f\left(\varepsilon^p\right) = \left(\varepsilon^p + \frac{\sigma_Y}{E}\right)^N$. The rate sensitivity exponent m also comes into play in (2.13). The dislocation properties of the material include the Burgers vector b and the coefficient α in the Taylor dislocation model.

Figures 4a and 4b show the distribution of hoop stress $\sigma_{\theta\theta}$ ahead of the crack tip on the plane $\theta = 0$. The stress distribution in classical plasticity (without the strain gradient effect) is also shown for comparison. The hoop stress is normalized by the tensile yield stress σ_Y. The distance r to the crack tip ranges from 0.1 μm to 200 μm, where 0.1 μm corresponds to the lower limit of CMSG, as discussed in Section 2.6. The material parameters are $\sigma_Y = 0.2\%E$, Poisson's ratio $\nu = 0.3$, plastic work hardening exponent $N = 0.2$, rate sensitivity exponent $m = 20$, Burgers vector $b = 0.255$ nm, and coefficient $\alpha = 0.5$ which is within the range (0.3 to 0.5) for the Taylor dislocation model. These give the intrinsic material length in (2.7) as $l = 3.53$ μm. The stress intensity factor in the remote elastic field is $K_I = 17.3\sigma_Y l^{1/2}$. For a representative yield stress $\sigma_Y = 200$ MPa, the remote stress intensity factor is $K_I = 6.5\ \text{MPa}\sqrt{m}$. It is observed from Figure 4a that CMSG and classical plasticity predict essentially the same stress distribution away from the crack tip. Within a zone of approximately 1 μm (at this stress intensity factor $K_I = 17.3\sigma_Y l^{1/2}$, CMSG gives a much higher stress level than the HRR field (Hutchinson, 1968; Rice and Rosengren, 1968) in classical plasticity. In fact, the stress level in CMSG is $12\sigma_Y$ at a distance of 0.1 μm to the crack tip. This stress level is high enough to trigger cleavage cracking, as discussed in Section 1. On the contrary, the stress level at the same distance 0.1 μm to the crack tip in classical plasticity is $7.5\sigma_Y$. The significant increase in stress is due to the strain gradient effect around the crack tip. To illustrate the transition from the remote elastic K field through the HRR field to the new stress field around the crack tip, we have shown the same stress distribution in Figure 4b but in the log-log scale. The curve for large r becomes a straight line with the slope $-1/2$, which corresponds to the elastic K field. The curve for r between 2 and 20 μm becomes another straight line with the slope $-N/(N+1)$, which corresponds to the HRR field (Hutchinson, 1968; Rice and Rosengren, 1968) in classical plasticity. The stress field predicted by CMSG agrees with the elastic K field and the HRR field in the corresponding regions, but becomes much larger within 1 μm distance to the crack tip.

We have also compared the stress distribution in Figure 4 to the higher-order theory of mechanism-based strain gradient plasticity (see Jiang et al., 2001). CMSG and the higher-order theory give identical stress distributions at a distance 0.1 μm away from the crack tip.

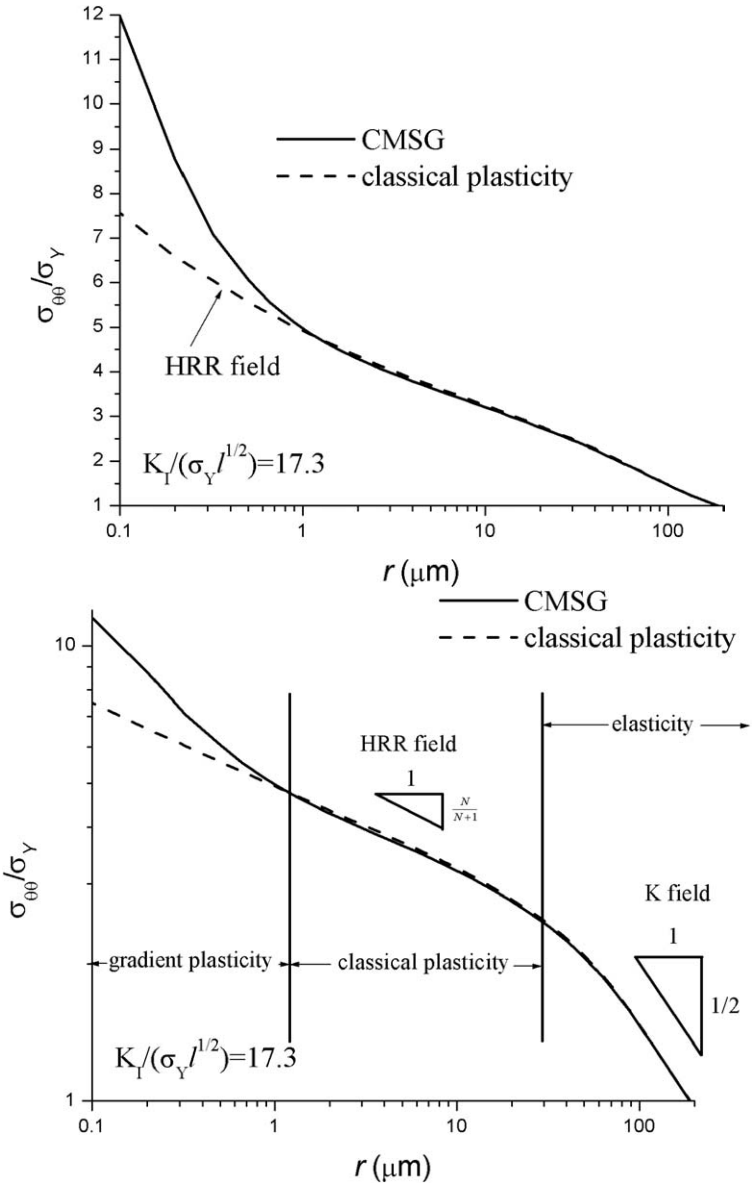

Figure 4. Distributions of the hoop stress $\sigma_{\theta\theta}$ ahead of the crack tip on the plane $\theta = 0$ in a homogeneous material predicted by the conventional theory of mechanism-based strain gradient plasticity (CMSG) and classical plasticity theory. Here r is the distance to the crack tip. The material properties include the Poisson's ratio $\nu = 0.3$, yield stress $\sigma_Y = 0.2\%$ (E is the Young's modulus), plastic working hardening exponent $N = 0.2$, rate sensitivity exponent $m = 20$, Burgers vector $b = 0.255$ nm, and the coefficient $\alpha = 0.5$ in the Taylor dislocation model. The stress intensity factor in the remote elastic field is $K_I = 17.3\sigma_Y l^{1/2}$, where $l = 3.53\ \mu m$ is the intrinsic material length in (2.7). a) The distance to the crack tip r is in log scale; b) Both $\sigma_{\theta\theta}$ and r are in log scale.

Table 1. Elastic properties of Sapphire, Alumina, Single Crystal Nb and Polycrystalline Nb (Korn et al., 2002)

	Young's modulus E (GPa)	Poisson's ratio ν
Sapphire	425	0.16
Alumina	390	0.27
Single Crystal Nb	145	0.36
Polycrystalline Nb	105	0.39

Figures 5a, b and c show the contour plots of the densities ρ_G and ρ_S of geometrically necessary dislocations and statistically stored dislocations, and the total dislocation density $\rho = \rho_G + \rho_S$. Here ρ_G and ρ_S are related to the effective plastic strain gradient and the uniaxial stress-plastic strain relation by $\rho_G = \bar{r}\eta^p/b$ and $\rho_S = \left[\sigma_{ref} f\left(\varepsilon^p\right)/(M\alpha\mu b)\right]^2$, respectively. The contours are shown in a region of 16 $\mu m \times 20$ μm surrounding the crack tip. The density ρ_G of geometrically necessary dislocations is large around the crack tip, but it rapidly decreases away from the crack tip. On the contrary, the density ρ_S of statistically stored dislocations is not as large as ρ_G around the crack tip, but it decreases much slower than ρ_G away from the crack tip. The contours of total dislocation density ρ in Figure 5c are similar to those of statistically stored dislocation density ρ_S in Figure 5b except in the immediate neighborhood of the crack tip. This suggests that both ρ_S and ρ_G are important near the crack tip, which is consistent with the conclusion established from Figure 4 that the significant increase in stress near the crack tip is due to the geometrically necessary dislocations.

Figure 6 shows the ratio of normal stress predicted by CMSG and by classical plasticity, $\sigma_{\theta\theta}^{CMSG}/\sigma_{\theta\theta}^{\text{classical}}$, at a distance $r = 0.1$ μm ahead of the crack tip ($\theta = 0$) versus the normalized stress intensity factor $KI/\left(\sigma_Y l^{1/2}\right)$. This ratio $\sigma_{\theta\theta}^{CMSG}/\sigma_{\theta\theta}^{\text{classical}}$ represents the stress increase due to the strain gradient effect. At a relatively small remote stress intensity factor $K_I = 17.3\sigma_Y l^{1/2}$, the stress accounting for the strain gradient effect is approximately 60% higher than that in classical plasticity. As the remote stress intensity factor K_I increases, the strain gradient effect becomes much more significant and the stress in CMSG can be almost 4 times that in classical plasticity.

4. Fracture of bimaterial interfaces

We use CMSG to investigate fracture of interfaces between elastic and elastic-plastic solids. To the best of our knowledge there exists no prior studies of the strain gradient effect on fracture of bimaterial interfaces. The focus of the present study is on the stress level near an interface crack tip in order to explore whether it is high enough to trigger cleavage cracking in presence of significant plastic flow as observed in Elssner et al.'s (1994) and Korn et al.'s (2002) experiments. Figure 7 shows a schematic diagram of the four-point bend specimen used in their experiments. A single crystal sapphire layer is sandwiched between a single crystal and a polycrystalline Nb layer, which in turn are sandwiched by two alumina layers. There is a notch on the interface between the single crystal Nb and sapphire, and the notch length is 0.4 mm. The inner span of the four-point bend specimen is 9 mm, and the momentum arm is also 9 mm (Figure 7). The specimen thickness (in the out-of-plane direction) is 2 mm.

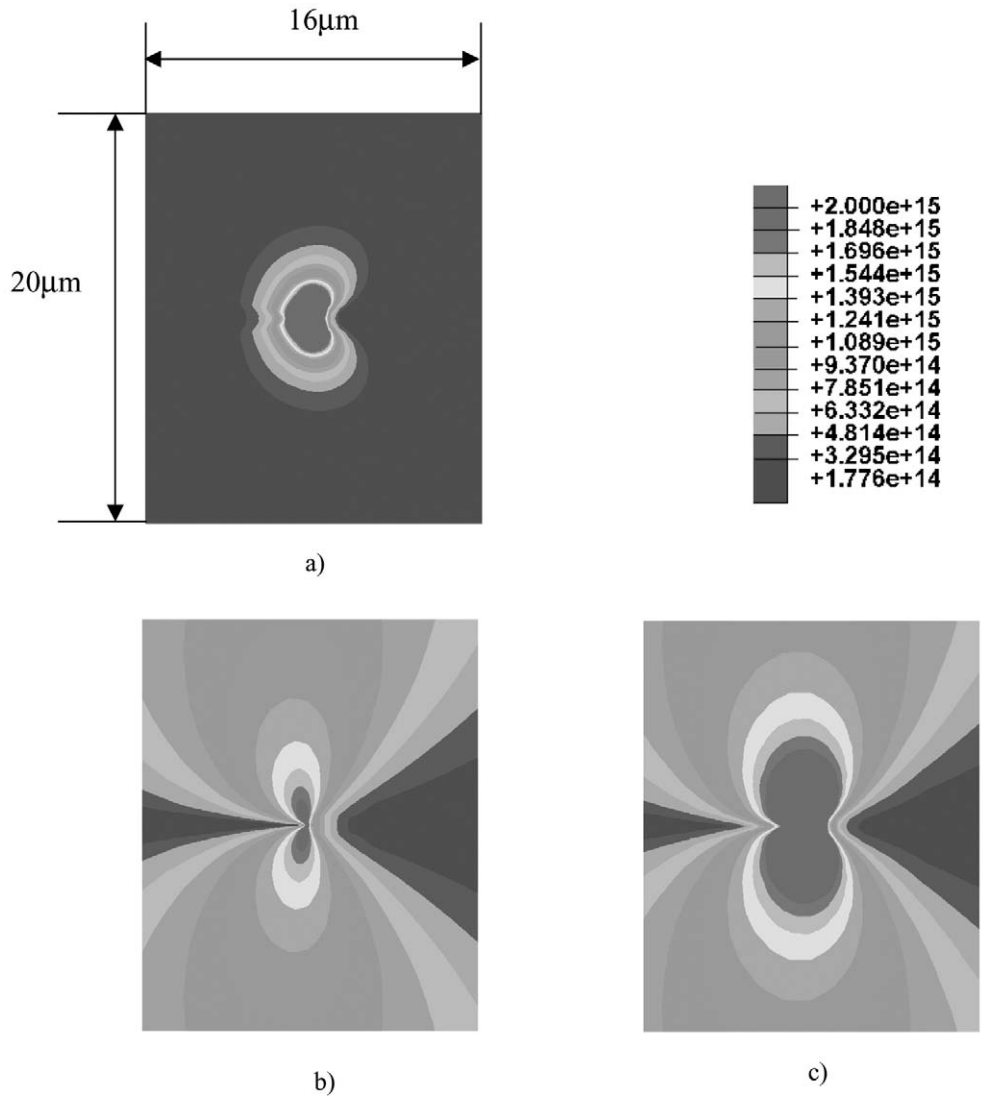

Figure 5. Contour plots of dislocation densities. a) geometrically necessary dislocation density ρ_G; b) statistically stored dislocation density ρ_S; c) total dislocation density $\rho = \rho_S + \rho_G$. The unit of dislocation densities is m^2. The material properties and the remote stress intensity factor are the same as those in Figure 4.

The four-point bend specimen in Figure 7 is analyzed by the two-dimensional, plane-strain finite element method. The finite element mesh is shown in Figure 8. The applied loads are imposed at the location shown in Figure 7. Sapphire and alumina are linear elastic. Their elastic properties, as well as those of single crystal and polycrystalline Nb, are given in Table 1 (Korn et al., 2002). The single crystal and polycrystalline Nb are both elastic-plastic with the uniaxial stress-plastic strain relation in (3.1). For single crystal Nb, we have taken the ratio of yield stress to Young's modulus as $\sigma_Y/E = 0.1\%$, which gives the yield stress $\sigma_Y = 145$ MPa. The plastic work hardening exponent is $N = 0.05$ to represent easy glide in single crystal deformation. For polycrystalline Nb, the plastic work hardening exponent $N = 0.24$ and the yield stress $\sigma_Y = 105$ MPa (http://www.rembar.com/niobium.htm), and the latter also gives the ratio of yield stress to Young's modulus $\sigma_Y/E = 0.1\%$. The rate sensitivity of Nb $m = 20$,

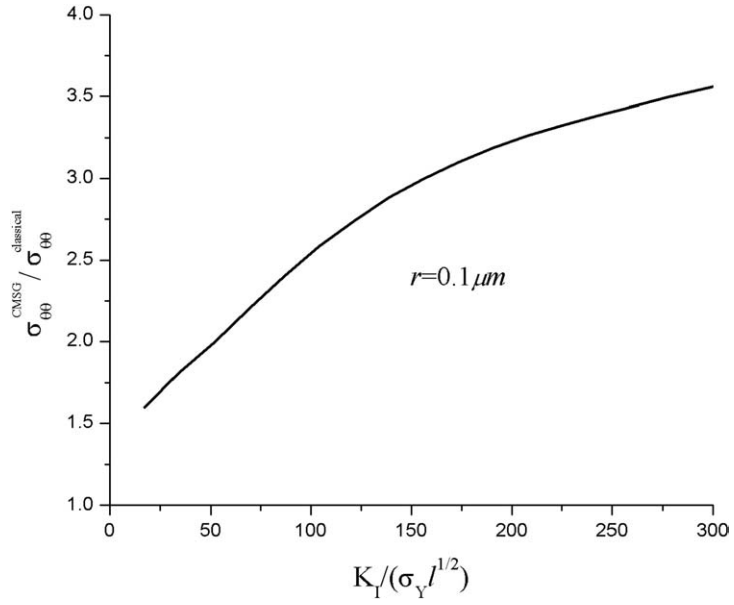

Figure 6. The ratio of normal stress predicted by CMSG and classical plasticity theories at a distance $r = 0.1$ μm ahead of the crack tip ($\theta = 0$) versus the normalized stress intensity factor $K_I / \left(\sigma_Y l^{1/2}\right)$. The material properties are the same as those in Figure 4.

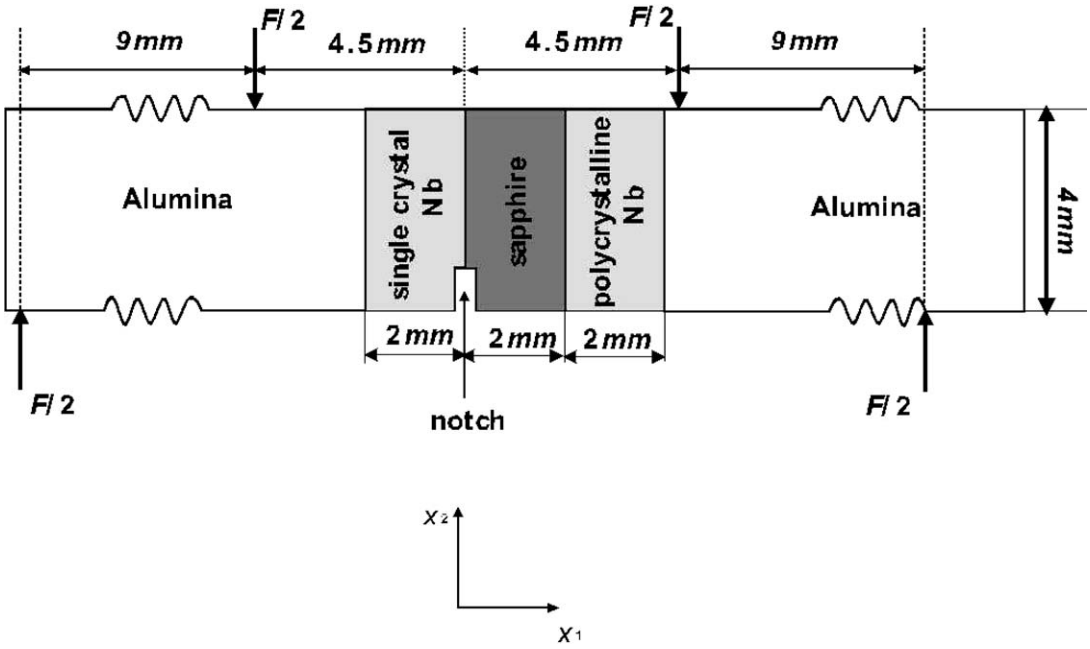

Figure 7. A schematic diagram of the four-point bend specimen used in Elssner et al.'s (1994) and Korn et al.'s (2002) experiments to study fracture of Nb/sapphire interface.

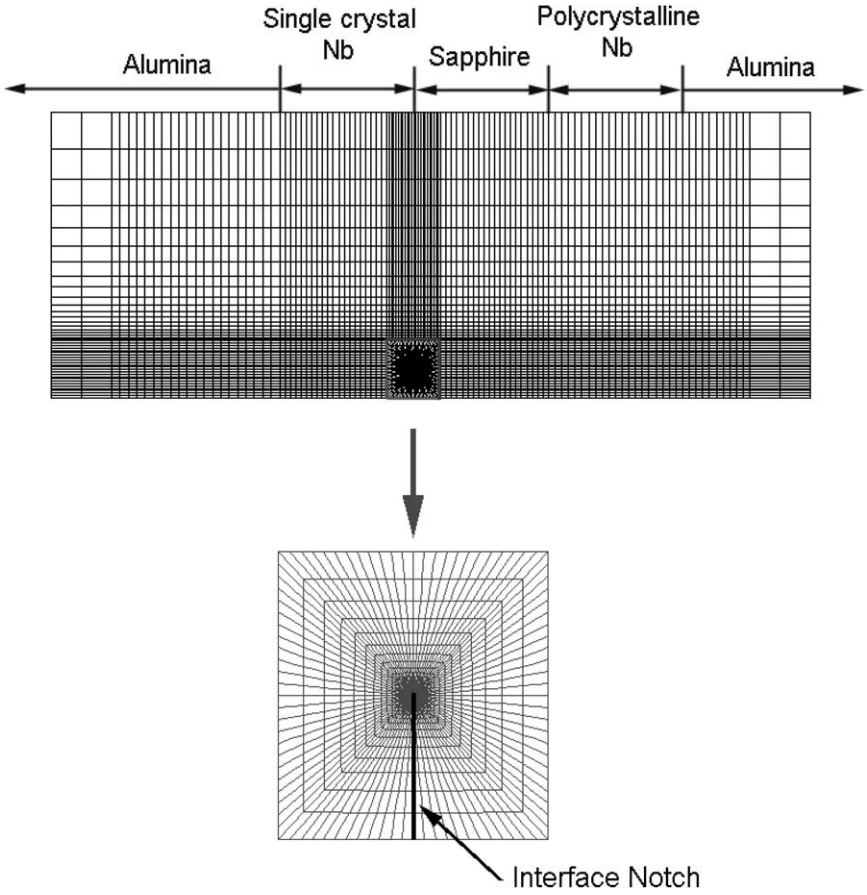

Figure 8. The finite element mesh for the four-point bend specimen shown in Figure 7.

Burgers vector $b = 0.25$ nm, and coefficient $\alpha = 0.5$ in the Taylor dislocation model. These give the intrinsic material length for Nb as $l = 5.29$ μm.

Figure 9 shows the distributions of normal stress σ_{11} and shear stress σ_{12} along the single crystal Nb/sapphire interface ahead of the notch tip. Here σ_{11} is the tensile stress normal to the interface. Both σ_{11} and σ_{12} are normalized by the yield stress $\sigma_Y = 145$ MPa of the single crystal Nb. The distance r to the notch tip ranges from 0.1 μm to 200 μm. The applied force is $F = 85N$. The shear stress σ_{12} is much smaller than the normal stress σ_{11} such that the tensile stress dominates at the interface crack tip (Figure 9 shows $-\sigma_{12}$ instead of σ_{12}.). This is because the sapphire layer is sandwiched between two Nb layers such that the mode mixity for the interface crack tip is small. Both CMSG and classical plasticity results are shown, and they give essentially the same stress distribution at a distance of more than 1 μm to the notch tip. For $r < 1$ μm, CMSG gives much higher normal stress than classical plasticity due to the strain gradient effect. In fact, classical plasticity gives $\sigma_{11} = 3.6\sigma_Y$ at $r = 0.1$ μm which is far short to trigger cleavage cracking. CMSG gives $\sigma_{11} = 13.3\sigma_Y$ at the same r. This stress is nearly 4 times that of classical plasticity, and definitely exceeds the stress needed for cleavage cracking. The stress increase around an interface crack tip (Figure 9) is much more drastic than that around a crack tip in a homogeneous solid (Figure 4). Therefore, CMSG provides an explanation of cleavage cracking along the bimaterial interface in presence of plastic flow.

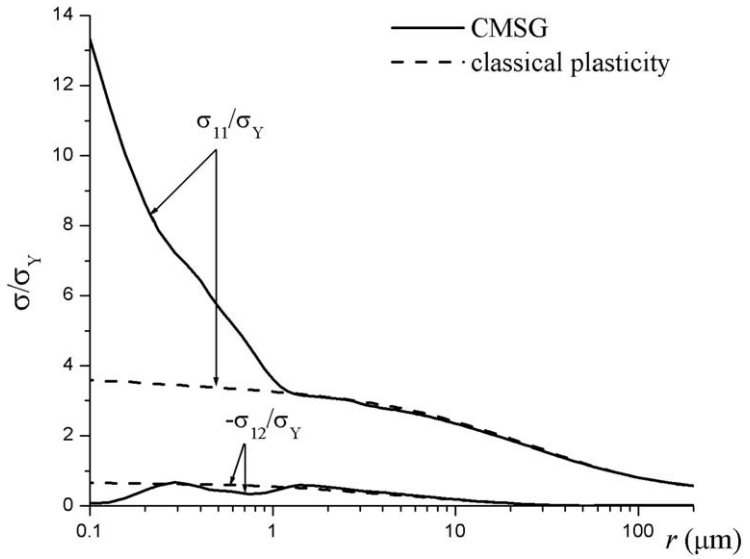

Figure 9. Distributions of normal stress σ_{11} and shear stress σ_{12} along the interface between the single crystal Nb and sapphire ahead of the notch tip, where σ_{11} is the tensile stress normal to the interface and σ_{11} and σ_{12} are normalized by the yield stress σ_Y of single crystal Nb. The elastic properties of sapphire, alumina, single crystal and polycrystalline Nb are given in Table 1. The ratio of yield stress to Young's modulus is 0.1% for both single crystal and polycrystalline Nb. The plastic work hardening exponent $N = 0.24$ and 0.05 for polycrystalline and single crystal Nb, respectively. The rate sensitivity exponent $m = 20$, Burgers vector $b = 0.25$ nm, and coefficient $\alpha = 0.5$ in the Taylor dislocation model. The applied force (see Figure 7) is $F = 85N$.

5. Concluding remarks

We have used the conventional theory of mechanism-based strain gradient plasticity (CMSG) (Huang et al., 2004) to investigate fracture of materials and bimaterial interfaces. CMSG is a lower-order theory of strain gradient plasticity established from the Taylor dislocation model (1934, 1938). Except in a thin boundary layer whose thickness is on the order of 10 nm, CMSG gives the same stress (or strain) field as the higher-order theory of mechanism-based strain gradient plasticity (Gao et al., 1999b; Huang et al., 2000a, b). The following conclusions are established in the present study.

(1) The stress level given by CMSG is much higher than that predicted by classical plasticity within a zone on the order of microns around the crack tip. Our finite element analysis clearly shows the transition from the remote elastic K field via the HRR field (Hutchinson, 1968; Rice and Rosengren, 1968) in classical plasticity to the new crack tip field.

(2) The contour plots of the dislocation densities clearly show that both geometrically necessary dislocations and statistically stored dislocations are important around the crack tip. The strain gradient effect associated with geometrically necessary dislocations is responsible for the significant stress increase around the crack tip.

(3) The stress increase due to the strain gradient effect around the crack tip at the Nb/sapphire interface is much more significant than that around a crack tip in a homogeneous material. The normal stress given by CMSG reaches 13.3 times the yield stress σ_Y of Nb at a distance 0.1 μm to the crack tip, while the classical plasticity theory (without the strain gradient effect) only gives a normal stress $3.6\sigma_Y$ at the same distance.

(4) This stress level ($13.3\sigma_Y$) due to the strain gradient effect is high enough to trigger cleavage cracking. Therefore, CMSG provides an explanation of cleavage fracture in presence of significant plastic flow observed in Elssner et al.'s (1994) and Korn et al.'s (2002) experiments for the Nb/sapphire bimaterial system.

6. Acknowledgements

Y.H. acknowledges the support from NSF (grant # CMS-0084980), ONR (grant # N00014-01-1-0205, program officer Dr Y.D.S. Rajapakse), and ASCI Center for Simulation of Advanced Rockets at the University of Illinois supported by US department of Energy through the University of California under subcontract B523819. The support from NSFC is also acknowledged.

References

Acharya, A. and Bassani, J.L. (2000). Lattice incompatibility and a gradient theory of crystal plasticity. *Journal of the Mechanics and Physics of Solids* **48**, 1565–1595.

Acharya, A. and Beaudoin, A.J. (2000). Grain-size effect in viscoplastic polycrystals at moderate strains. *Journal of the Mechanics and Physics of Solids* **48**, 2213–2230.

Argon, A.S., Seleznev, M.L., Shih, C.F. and Liu, X.H. (1998). Role of controlled debonding along fiber/matrix interfaces in the strength and toughness of metal matrix composites. *International Journal of Fracture* **93**, 351–371.

Arsenlis, A. and Parks, D.M. (1999). Crystallographic aspects of geometrically-necessary and statistically-stored dislocation density. *Acta Materialia* **47**, 1597–1611.

Asaro, R.J. and Needleman, A. (1985). Texture development and strain hardening in rate dependent polycrystals. *Acta Metallurgica et Materialia* **33**, 923–953.

Ashby, M.F. (1970). The deformation of plastically non-homogeneous alloys. *Philosophical Magazine* **21**, 399–424.

Atkinson, M. (1995). Further analysis of the size effect in indentation hardness tests of some metals. *Journal of Materials Research* **10**, 2908–2915.

Bagchi, A. and Evans, A.G. (1996). The mechanics and physics of thin film decohesion and its measurement. *Interface Science* **3**, 169–193.

Bagchi, A., Lucas, G.E., Suo, Z. and Evans, A.G. (1994). A new procedure for measuring the decohesion energy of thin ductile films on substrates. *Journal of Materials Research* **9**, 1734–1741.

Bailey, J.E. and Hirsch, P.B. (1960). The dislocation distribution, flow stress, and stored energy in cold-worked polycrystalline silver. *Philosophical Magazine* **5**, 485–497.

Bassani, J.L. (2001). Incompatibility and a simple gradient theory of plasticity. *Journal of the Mechanics and Physics of Solids* **49**, 1983–1996.

Beaudoin, A.J. and Acharya, A. (2001). A model for rate-dependent flow of metal polycrystals based on the slip plane lattice incompatibility. *Materials Science and Engineering A* **309**, 411–415.

Beltz, G.E. and Wang, J.S. (1992). Crack direction effects along copper sapphire interfaces. *Acta Metallurgica et Materialia* **40**, 1675–1683.

Beltz G.E., Rice, J.R., Shih, C.F. and Xia, L. (1996). A self-consistent method for cleavage in the presence of plastic flow. *Acta Materialia* **44**, 3943–3954.

Bilby, B.A., Bullough, R. and Smith, E. (1955). Continuous distributions of dislocation: a new application of the methods of non-Riemannian geometry. *Proceedings of the Royal Society of London A* **231**, 263–273.

Bishop, J.F.W. and Hill, R. (1951a). A theory of plastic distortion of a polycrystalline aggregate under combined stresses. *Philosophical Magazine* **42**, 414–427.

Bishop, J.F.W. and Hill, R. (1951b). A theoretical derivation of the plastic properties of a polycrystalline face-centered metal. *Philosophical Magazine* **42**, 1298–1307.

Camacho, G.T. and Ortiz, M. (1996). Computational modeling of impact damage in brittle materials. *International Journal of Solids and Structures* **33**, 2899–2938.

Canova, G.R. and Kocks, U.F. (1984). The development of deformation textures and resulting properties of fcc metals. In C.M. Brakman, P. Jongenburger and E.J. Mittemeijer (eds.) *Seventh Int. Conf. on Textures of Materials. Soc. for Materials Science*. Netherlands (1984) pp. 573–579.

Cermelli, P. and Gurtin, M.E. (2001). On the characterization of geometrically necessary dislocations in finite plasticity. *Journal of the Mechanics and Physics of Solids* **49**, 1539–1568.

Chen, J.Y., Huang, Y. and Hwang, K.C. (1998). Mode I and Mode II plane-stress near-tip fields for cracks in materials with strain gradient effect. *Key Engineering Materials* **145**, 19–28.

Chen, J.Y., Wei, Y., Huang, Y., Hutchinson, J.W. and Hwang, K.C. (1999). The crack tip fields in strain gradient plasticity: the asymptotic and numerical analyses. *Engineering Fracture Mechanics* **64**, 625–648.

Cottrell, A.H. (1964). *The mechanical Properties of Materials*. J. Willey, New York p. 277.

Dai, H. and Parks, D.M. (2003). Geometrically-necessary dislocation density in continuum crystal plasticity theory and FEM implementation. Unpublished manuscript.

De Guzman, M.S., Neubauer, G., Flinn, P. and Nix, W.D. (1993). The role of indentation depth on the measured hardness of materials. *Materials Research Symposium Proceedings* **308**, 613–618.

Douglass, M.R. (1998). Lifetime estimates and unique failure mechanisms of the digital micromirror device (DMD). *Annual Proceedings-Reliability Physics Symposium* (Sponsored by IEEE), Mar 31-Apr 2, 1998, 9–16; also http://www.dlp.com/dlp/resources/whitepapers/pdf/ieeeir.pdf.

Elssner, G., Korn, D. and Rühle, M. (1994). The influence of interface impurities on fracture energy of UHV diffusion-bonded metal-ceramic bicrystals. *Scripta Metallurgica et Materialia* **31**, 1037–1042.

Eshelby, J.D. (1956). The continuum theory of lattice defects. In F.D. Seitz and D. Turnbull (eds.) *Solid State Physics*, Vol. 3. Academic Press, New York pp. 79–144.

Evers, L.P., Parks, D.M., Brekelmans, W.A.M. and Geers, M.G.D. (2002). Crystal plasticity model with enhanced hardening by geometrically necessary dislocation accumulation. *Journal of the Mechanics and Physics of Solids* **50**, 2403–2424.

Fleck, N.A. and Hutchinson, J.W. (1993). A phenomenological theory for strain gradient effects in plasticity. *Journal of the Mechanics and Physics of Solids* **41**, 1825–1857.

Fleck, N.A., Muller, G.M., Ashby, M.F. and Hutchinson J.W. (1994). Strain gradient plasticity: theory and experiments. *Acta Metallurgica et Materialia* **42**, 475–487.

Fleck, N.A. and Hutchinson, J.W. (1997). Strain gradient plasticity. In J.W. Hutchinson and T.Y. Wu (eds.) *Advances in Applied Mechanics*, Vol. 33. Academic Press, New York pp. 295–361.

Fleck, N.A. and Hutchinson, J.W. (2001). A reformulation of strain gradient plasticity. *Journal of the Mechanics and Physics of Solids* **49**, 2245–2271.

Fox, N. (1966). A continuum theory of dislocations for single crystals. *Journal of Institute for Mathematics and its Applications* **2**, 285–298.

Gao, H., Huang, Y. and Nix, W.D. (1999a). Modeling plasticity at the micrometer scale. *Naturwissenschaften* **86**, 507–515.

Gao, H., Huang, Y., Nix, W.D. and Hutchinson, J.W. (1999b). Mechanism-based strain gradient plasticity - I. Theory. *Journal of the Mechanics and Physics of Solids* **47**, 1239–1263.

Gurtin, M.E. (2002). A gradient theory of single-crystal viscoplasticity that accounts for geometrically necessary dislocations. *Journal of the Mechanics and Physics of Solids* **50**, 5–32.

Haque, M.A. and Saif, M.T.A. (2003). Strain gradient effect in nanoscale thin films. *Acta Materialia* **51**, 3053–3061.

Huang, Y., Zhang, L., Guo, T.F. and Hwang, K.C. (1995). Near tip fields for cracks in materials with strain-gradient effect. In J.R. Willis (ed.) *Proceedings of IUTAM Symposium on Nonlinear Analysis of Fracture*. Kluwer Academic Publishers, Cambridge, England pp. 231–242.

Huang, Y., Zhang, L., Guo, T.F. and Hwang, K.C. (1997). Mixed mode near-tip fields for cracks in materials with strain gradient effects. *Journal of the Mechanics and Physics of Solids* **45**, 439–465.

Huang, Y., Chen, J.Y., Guo, T.F., Zhang, L. and Hwang, K.C. (1999). Analytical and numerical studies on mode I and mode II fracture in elastic-plastic materials with strain gradient effects. *International Journal of Fracture* **100**, 1–27.

Huang, Y., Gao, H., Nix, W.D. and Hutchinson, J.W. (2000a). Mechanism-based strain gradient plasticity - II. Analysis. *Journal of the Mechanics and Physics of Solids* **48**, 99–128.

Huang, Y., Xue, Z., Gao, H., Nix, W.D. and Xia, Z.C. (2000b). A study of microindentation hardness tests by mechanism-based strain gradient plasticity. *Journal of Materials Research* **15**, 1786–1796.

Huang, Y., Qu, S., Hwang, K.C., Li, M. and Gao, H. (2004). A conventional theory of mechanism-based strain gradient plasticity. *International Journal of Plasticity* **20**, 753–782.

Hutchinson, J.W. (1968). Singular behavior at the end of a tensile crack in a hardening material. *Journal of the Mechanics and Physics of Solids* **16**, 13–31.

Hutchinson, J.W. (1976). Bounds and self-consistent estimates for creep of polycrystalline materials. *Proceedings of the Royal Society of London A* **348**, 101–127.

Hutchinson, J.W. (1997). Linking scales in mechanics. In B.L. Karihaloo, Y.W. Mai, M.I. Ripley and R.O. Ritchie (eds.) *Advances in Fracture Research*. Pergamon Press, Amsterdam pp. 1–14.

Hwang, K.C., Jiang, H., Huang, Y., Gao, H. and Hu, N. (2002). A finite deformation theory of strain gradient plasticity. *Journal of the Mechanics and Physics of Solids* **50**, 81–99.

Hwang, K.C., Jiang, H., Huang, Y. and Gao, H. (2003). Finite deformation analysis of mechanism-based strain gradient plasticity: torsion and crack tip field. *International Journal of Plasticity* **19**, 235–251.

Jiang, H., Huang, Y., Zhuang, Z. and Hwang, K.C. (2001). Fracture in mechanism-based strain gradient plasticity. *Journal of the Mechanics and Physics of Solids* **49**, 979–993.

Kocks, U.F. (1970). The relation between polycrystal deformation and single crystal deformation. *Metallurgical and Materials Transactions* **1**, 1121–1144.

Kok, S., Beaudion, A.J. and Tortorelli, D.A. (2002a). A polycrystal plasticity model based on the mechanical threshold. *International Journal of Plasticity* **18**, 715–741.

Kok, S., Beaudoin, A.J. and Tortorelli, D.A. (2002b). On the development of stage IV hardening using a model based on the mechanical threshold. *Acta Materialia* **50**, 1653–1667.

Kok, S., Beaudoin, A.J., Tortorelli, D.A. and Lebyodkin, M. (2002c). A finite element model for the Portevin-Le Chatelier effect based on polycrystal plasticity. *Modelling and Simulation in Materials Science and Engineering* **10**, 745–763.

Kondo, K. (1952). On the geometrical and physical foundations of the theory of yielding. *Proceedings Japan National Congress of Applied Mechanics* **2**, 41–47.

Kondo, K. (1955). Non-Riemannian geometry of imperfect crystals from a macroscopic viewpoint. In K. Kondo (ed.) *RAAG Memoirs of the Unifying Study of Basic Problems in Engineering and Physical Science by Means of Geometry*, Vol. 1. Gakuyusty Bunken Fukin-Kay, Tokyo.

Korn, D., Elssner, G., Fischmeister, H.F. and Rühle, M. (1992). Influence of interface impurities on the fracture energy of UHV bonded niobium sapphire bicrystals. *Acta Metallurgica et Materialia* **40**, S355–S360. Suppl. S.

Korn, D., Elssner, G., Cannon, R.M. and Rühle, M. (2002). Fracture properties of interfacially doped Nb-Al_2O_3 bicrystals: I, fracture characteristics. *Acta Materialia* **50**, 3881–3901.

Kröner, E. (1960). Allgemeine kontinuumstheorie der Versetzungen und Eigenspannungen. *Archive for Rational Mechanics and Analysis* **4**, 273–334.

Lee, E.H. (1969). Elastic-plastic deformation at finite strains. *Journal of Applied Mechanics* **36**, 1–6.

Lloyd, D.J. (1994). Particle reinforced aluminum and magnesium matrix composites. *International Materials Reviews* **39**, 1–23.

Lou, J., Shrotriya, P., Buchheit, T., Yang, D and Soboyejo, W.O. (2003). Nanoindentation study of plasticity length scale effects in LIGA Ni microelectromechanical systems structures. *Journal of materials Research* **18**, 719–728.

Ma, Q. and Clarke, D.R. (1995). Size dependent hardness of silver single crystals. *Journal of Materials Research* **10**, 853–863.

McElhaney, K.W., Vlasssak, J.J. and Nix, W.D. (1998). Determination of indenter tip geometry and indentation contact area for depth-sensing indentation experiments. *Journal of Materials Research* **13**, 1300–1306.

Mindlin, R.D. (1964). Micro-structure in linear elasticity. *Archive Rational Mechanics Analysis* **16**, 51–78.

Needleman, A. (1987). A continuum model for void nucleation by inclusion debonding. *Journal of Applied Mechanics* **54**, 525–531.

Needleman, A. and van der Giessen, E. (2001). Discrete dislocation and continuum descriptions of plastic flow. *Material Science and Engineering A* **309**, 1–13.

Nix, W.D. (1989). Mechanical properties of thin films. *Materials Transactions* **20A**, 2217–2245.

Nix, W.D. (1997). Elastic and plastic properties of thin films on substrates: nanoindentation techniques. *Materials Science and Engineering A* **234**, 37–44.

Nix, W.D. and Gao, H. (1998). Indentation size effects in crystalline materials: A law for strain gradient plasticity. *Journal of the Mechanics and Physics of Solids* **46**, 411–425.

Nye, J.F. (1953). Some geometrical relations in dislocated crystals. *Acta Metallurgica et Materialia* **1**, 153–162.
O'Dowd, N.P., Stout, M.G. and Shih, C.F. (1992). Fracture-toughness of alumina niobium interfaces-experiments and analyses. *Philosophical Magazine A* **66**, 1037–1064.
Oh, T.S., Cannon, R.M. and Ritchie, R.O. (1987). Subcritical crack growth along ceramic-metal interfaces. *Jom-Journal of the Minerals, Metals and Materials Society* **39**, A57–A57.
Poole, W.J., Ashby, M.F. and Fleck, N.A. (1996). Micro-hardness of annealed and work-hardened copper polycrystals. *Scripta Materialia* **34**, 559–564.
Qiu, X., Huang, Y., Nix, W.D., Hwang, K.C. and Gao, H. (2001). Effect of intrinsic lattice resistance in strain gradient plasticity. *Acta Materialia* **49**, 3949–3958.
Qiu, X., Huang, Y., Wei, Y., Gao, H. and Hwang, K.C. (2003). The flow theory of mechanism-based strain gradient plasticity. *Mechanics of Materials* **35**, 245–258.
Rice, J.R. and Rosengren, G.F. (1968). Plane strain deformation near a crack tip in a power law hardening material. *Journal of the Mechanics and Physics of Solids* **16**, 1–12.
Saha, R., Xue, Z., Huang, Y. and Nix, W.D. (2001). Indentation of a soft metal film on a hard substrate: strain gradient hardening effects. *Journal of the Mechanics and Physics of Solids* **49**, 1997–2014.
Shi, M., Huang, Y., Gao, H. and Hwang, K.C. (2000a). Non-existence of separable crack tip field in mechanism-based strain gradient plasticity. *International Journal of Solids and Structures* **37**, 5995–6010.
Shi, M., Huang, Y. and Hwang, K.C. (2000b). Fracture in the higher-order elastic continuum. *Journal of the Mechanics and Physics of Solids* **48**, 2513–2538.
Shi, M., Huang, Y., Jiang, H., Hwang, K.C. and Li, M. (2001). The boundary-layer effect on the crack tip field in mechanism-based strain gradient plasticity. *International Journal of Fracture* **112**, 23–41.
Shi, M., Huang, Y. and Gao, H. (2004a). The J-integral and geometrically necessary dislocations in nonuniform plastic deformation. *International Journal of Plasticity* **20**, 1739–1762.
Shi, M., Huang, Y., Li, M. and Hwang, K.C. (2004b). On source-limited dislocations in nanoindentation. *Journal of Applied Mechanics* (ASME Transactions) (in press).
Shizawa, K. and Zbib, H.M. (1999). A thermodynamical theory of gradient elastoplasticity with dislocation density tensor. I: Fundamentals. *International Journal of Plasticity* **15**, 899–938.
Shrotriya, P., Allameh, S.M., Lou, J., Buchheit, T. and Soboyejo, W.O. (2003). On the measurement of the plasticity length scale parameter in LIGA nickel foils. *Mechanics of Materials* **35**, 233–243.
Steinmann, P. (1996). Views on multiplicative elastoplasticity and the continuum theory of dislocations. *International Journal of Engineering Science* **34**, 1717–1735.
Stelmashenko, N.A., Walls, A.G., Brown, L.M. and Milman, Y.V. (1993). Microindentation on W and Mo oriented single crystals: an STM study. *Acta Metallurgica et Materialia* **41**, 2855–2865.
Stolken, J.S. and Evans, A.G. (1998). A microbend test method for measuring the plasticity length scale. *Acta Materialia* **46**, 5109–5115.
Suo, Z., Shih, C.F. and Varias, A.G. (1993). A theory for cleavage cracking in the presence of plastic flow. *Acta Metallurgica et Materialia* **41**, 1551–1557.
Suresh, S., Nieh, T.G. and Choi, B.W. (1999). Nano-indentation of copper thin films on silicon substrates. *Scripta Materialia* **41**, 951–957.
Swadener, J.G., George, E.P. and Pharr, G.M. (2002). The correlation of the indentation size effect measured with indenters of various shapes. *Journal of the Mechanics and Physics of Solids* **50**, 681–694.
Taylor, G.I. (1934). The mechanism of plastic deformation of crystals. Part I.–theoretical. *Proceedings of the Royal Society of London A* **145**, 362–387.
Taylor, G.I. (1938). Plastic strain in metals. *Journal of the Institute of Metals* **62**, 307–324.
Tvergaard, V. and Hutchinson, J.W. (1992). The relation between crack growth resistance and fracture process parameters in elastic-plastic solids. *Journal of the Mechanics and Physics of Solids* **40**, 1377–1397.
Tvergaard, V. and Hutchinson, J.W. (1993). The influence of plasticity on mixed mode interface toughness. *Journal of the Mechanics and Physics of Solids* **41**, 1119–1135.
Tymiak, N.I., Kramer, D.E., Bahr, D.F., Wyrobek, T.J. and Gerberich, W.W. (2001). Plastic strain and strain gradients at very small indentation depths. *Acta Materialia* **49**, 1021–1034.
van der Giessen, E., Deshpande, V.S., Cleveringa, H.H.M. and Needleman, A. (2001). Discrete dislocation plasticity and crack tip fields in single crystals. *Journal of the Mechanics and Physics of Solids* **49**, 2133–2153.
Volokh, K.Yu. and Hutchinson, J.W. (2002). Are lower-order gradient theories of plasticity really lower order? *Journal of Applied Mechanics* **69**, 862–864.

Wang, J.S. and Anderson, P.M. (1991). Fracture behavior of embrittled FCC metal bicrystals and its misorientation dependence. *Acta Metallurgica et Materialia* **39**, 779–792.

Wei, Y. and Hutchinson, J.W. (1997). Steady-state crack growth and work of fracture for solids characterized by strain gradient plasticity. *Journal of the Mechanics and Physics of Solids* **45**, 1253–1273.

Wei, Y. and Hutchinson, J.W. (1999). Models of interface separation accompanied by plastic dissipation at multiple scales. *International Journal of Fracture* **95**, 1–17.

Xia, Z.C. and Hutchinson, J.W. (1996). Crack tip fields in strain gradient plasticity. *Journal of the Mechanics and Physics of Solids* **44**, 1621–1648.

Xu, X.-P. and Needleman, A. (1994). Numerical simulations of fast crack growth in brittle solids. *Journal of the Mechanics and Physics of Solids* **42**, 1397–1434.

Yun, G., Qin, J., Huang, Y. and Hwang, K.C. (2004). A study of lower-order strain gradient plasticity theories by the method of characteristics. *European Journal of Mechanics A/Solids* (in press).